Research Square

Preprints are preliminary reports that have not undergone peer review.
They should not be considered conclusive, used to inform clinical practice,
or referenced by the media as validated information.

Multimodal MRI links brainstem susceptibility, sleep architecture, and glymphatic-related diffusion in Parkinson's disease

Aocai Yang
Shandong Provincial Hospital
Yuxin Li
Shandong Provincial Hospital
Yang Zhao
Shandong Provincial Hospital
Tao Gong
Shandong Provincial Hospital
Yufan Chen
Shandong Provincial Hospital
Lingyan Zhou
Shandong Provincial Hospital
Cheng Zhao
Shandong Provincial Hospital
Zhanfang Sun
Shandong Provincial Hospital
Yuanyuan Xiang
Shandong Provincial Hospital
Guangbin Wang
wgb79325960hotmail.com

Shandong Provincial Hospital

Article

Keywords:

Posted Date: September 20th, 2026

DOI: https://doi.org/10.21203/rs.3.rs-10799866/v1

License: This work is licensed under a Creative Commons Attribution 4.0 International License.
Read Full License

Additional Declarations: No competing interests reported.

Abstract

Background

Sleep disturbances are prevalent non-motor symptoms of Parkinson's disease (PD), yet their associations with brainstem imaging alterations and glymphatic-related diffusion processes remain inadequately elucidated. This study aimed to determine whether multimodal MRI markers of neuromelanin-containing brainstem nuclei correlate with objective sleep disturbances and diffusion tensor imaging analysis along the perivascular space (DTI-ALPS) in individuals with PD.

Methods

A cohort of thirty-four PD patients and twenty-seven healthy controls underwent multimodal MRI, including sub-voxel quantitative susceptibility mapping (QSM), neuromelanin-sensitive MRI (NM), and DTI-ALPS. Additionally, all PD patients participated in overnight polysomnography and were categorized into PD with sleep disturbance (PD-SD, n = 12) or PD without sleep disturbance (PD-NSD, n = 22) groups based on predefined polysomnography-derived criteria, such as prolonged sleep onset latency and/or increased apnea–hypopnea index.

Results

Compared with patients with PD-NSD, patients with PD-SD showed reduced REM sleep proportion, longer N1 sleep duration, and greater arousal burden. Voxel-wise analysis revealed higher absolute diamagnetic susceptibility ($|\chi_{dia}|$) in a substantia nigra cluster in PD-NSD than in PD-SD. ROI-based analyses identified distinct LC–SN imaging profiles across groups, including lower right LC paramagnetic susceptibility (χ_{para}) in PD-SD relative to healthy controls, higher $|\chi_{dia}|$ value of SNpc in PD-NSD, and reduced bilateral SNpc neuromelanin-sensitive contrast ratio in patients with PD. LC and SN imaging markers were associated with specific components of sleep architecture, including N3 and REM sleep. DTI-ALPS was associated with both N3 sleep percentage and LC χ_{para}, while NM ratio signal was inversely associated with χ_{para} value in SNpc. Multimodal imaging models showed higher apparent discriminative performance than individual imaging markers, particularly for distinguishing PD-SD from healthy controls.

Conclusion

The results indicate that sleep disturbances, as defined by polysomnography in PD, are associated with distinct imaging profiles of the locus coeruleus and substantia nigra, linked to iron redistribution, α-synuclein aggregation and loss of neuromelanin neuro, as well as glymphatic-related diffusion

alterations. These associations support a hypothesis-generating framework that links brainstem imaging alterations with sleep disturbances in PD.

1. Introduction

Parkinson's disease (PD) is a progressive neurodegenerative disorder, clinically characterized by bradykinesia, rigidity, resting tremor, and postural instability, and pathologically by the degeneration of dopaminergic neurons in the substantia nigra pars compacta (SNpc) along with the accumulation of misfolded α-synuclein[1]. While motor symptoms remain central to clinical diagnosis, non-motor manifestations are increasingly acknowledged as significant contributors to disease burden, clinical heterogeneity, and progression[2]. Among these non-motor symptoms, sleep disturbances are notably prevalent, affecting between 40% and 90% of patients throughout the disease trajectory. These disturbances include insomnia, sleep fragmentation, excessive daytime sleepiness, sleep-disordered breathing, and rapid eye movement (REM) sleep behavior disorder (RBD)[3]. Notably, several sleep abnormalities can precede the onset of motor symptoms by several years, with RBD now recognized as one of the most robust prodromal indicators of synucleinopathies[4]. Moreover, sleep disturbances have been linked to cognitive decline, autonomic dysfunction, reduced quality of life, and accelerated disease progression. Despite their clinical significance, the neurobiological mechanisms underlying sleep disturbances in PD remain incompletely understood.

Recent evidence indicates that degeneration of the locus coeruleus (LC) may serve as a critical underlying factor for sleep-related symptoms in PD[5]. The LC is the primary source of noradrenergic projections throughout the central nervous system and plays a pivotal role in regulating arousal, attention, autonomic function, and sleep-wake transitions. Through its extensive projections to cortical, limbic, thalamic, and brainstem regions, the LC is integral to the maintenance of wakefulness and the regulation of REM sleep[6]. Neuropathological studies suggest that LC involvement may occur early in the disease process, preceding significant nigrostriatal degeneration[5]. Notably, recent experimental research has demonstrated that the selective overexpression of human α-synuclein within LC noradrenergic neurons is sufficient to induce prodromal Parkinsonian phenotypes in mice, providing direct evidence that LC dysfunction may initiate non-motor manifestations prior to overt motor impairment. These findings suggest that sleep disturbances in PD may reflect early pathological changes within the LC and its associated brainstem networks.

Although LC pathology may manifest during the prodromal phase of PD, degeneration of the SN remains the defining pathological feature of the disorder[7]. In addition to its well-established role in motor control, the dopaminergic system is implicated in the regulation of arousal, sleep maintenance, and daytime alertness[8]. Notably, both the LC and SN are neuromelanin-containing nuclei within the brainstem that demonstrate selective vulnerability to α-synuclein pathology[9]. Emerging evidence indicates that these nuclei do not operate in isolation but rather as interconnected elements of a more extensive brainstem network involved in sleep–wake regulation. Consequently, degeneration within this

LC–SN network may contribute to alterations in objective sleep architecture[10]. Nonetheless, the extent to which sleep disturbances in PD are associated with concurrent abnormalities in both LC and SN integrity, and the relationship of these abnormalities to polysomnography-derived sleep architecture, remains inadequately understood.

Iron dyshomeostasis and neuromelanin depletion are increasingly acknowledged as critical pathological mechanisms contributing to the degeneration of the LC and SN[11]. The excessive accumulation of iron may facilitate oxidative stress, mitochondrial dysfunction, lipid peroxidation, and α-synuclein aggregation, thereby expediting neurodegenerative processes[12]. Conversely, neuromelanin typically serves as an intracellular metal-binding reservoir, capable of sequestering potentially toxic iron species[13]. The loss of neuromelanin-containing neurons may thus disrupt iron homeostasis and exacerbate neuronal damage. Consequently, iron deposition and neuromelanin depletion may constitute complementary pathological markers of brainstem degeneration in PD[14]. Quantitative susceptibility mapping (QSM) facilitates the *in vivo* evaluation of tissue magnetic susceptibility and has been extensively employed to assess iron-related changes in PD[15]. Recently, advanced susceptibility source-separation techniques, such as the Apparent Paramagnetic and Diamagnetic Component Quantitative Susceptibility Mapping (APART-QSM), have been developed to decompose total susceptibility into paramagnetic and diamagnetic components, thereby offering a more precise characterization of tissue composition[16, 17]. Neuromelanin-sensitive MRI (NM-MRI) offers complementary information regarding the integrity of catecholaminergic neurons within the LC and SN[18]. Together, these techniques provide a multimodal framework for characterizing brainstem degeneration in vivo.

Recent research has identified sleep as a crucial regulator of glymphatic function, a comprehensive brain-wide clearance mechanism that facilitates the exchange of cerebrospinal fluid and interstitial fluid along perivascular spaces[19]. This system enables the removal of metabolic waste products and neurotoxic proteins, including α-synuclein, from the brain parenchyma. Experimental studies have shown that glymphatic transport is enhanced during sleep, particularly during slow-wave sleep[20], while sleep fragmentation and deprivation diminish clearance efficiency. Considering the central role of the LC in regulating arousal and sleep–wake transitions, degeneration of the LC–SN network may indirectly affect glymphatic function by altering sleep architecture. Consequently, impaired glymphatic clearance associated with sleep has been proposed as a potential mechanism linking sleep disturbances to the progression of neurodegenerative diseases. Additionally, DTI-ALPS has recently been developed as a non-invasive MRI marker of glymphatic-related diffusion, demonstrating associations with sleep quality and neurodegenerative disorders[21]. However, whether glymphatic-related diffusion abnormalities are associated with both brainstem degeneration and objective sleep architecture in PD remains largely unknown.

In summary, accumulating evidence indicates that sleep disturbances in PD may originate from interconnected pathological processes, including the degeneration of neuromelanin-containing brainstem nuclei, disruption of sleep–wake regulatory networks, and impaired sleep-dependent brain

clearance mechanisms. However, these processes have predominantly been examined in isolation, with limited studies integrating objective polysomnography with multimodal MRI assessments of LC-SN integrity and glymphatic-related diffusion.

Consequently, the present study employed a combination of polysomnography, sub-voxel QSM, NM signal, and DTI-ALPS to investigate sleep disturbances in PD patients. By integrating objective evaluations of sleep architecture with multimodal assessments of LC-SN integrity and glymphatic-related diffusion, this study aimed to elucidate the relationships among brainstem degeneration, sleep architecture, and glymphatic-related diffusion in PD. This comprehensive approach may enhance our understanding of the biological mechanisms underlying sleep dysfunction and clarify how alterations in sleep-regulating brainstem nuclei are associated with sleep architecture and brain clearance pathways.

2. Materials and methods

2.1 Study design and participants

This prospective cross-sectional study was conducted at the Department of Neurology, Shandong Provincial Hospital Affiliated to Shandong First Medical University. Patients with early-stage Parkinson's disease (PD) were consecutively recruited between January 2023 and December 2024, and age- and sex-matched healthy controls (HCs) were recruited from the local community during the same period. The study protocol was approved by the institutional ethics committee, and written informed consent was obtained from all participants before enrollment.

Initially, a cohort of 50 patients diagnosed with PD and 35 HCs were recruited for the study. Within the PD cohort, nine individuals were excluded due to incomplete magnetic resonance imaging (MRI) examinations, and an additional seven were excluded owing to the lack of completed overnight polysomnography (PSG). Similarly, within the HC group, five participants were excluded because of incomplete MRI examinations, and three were excluded due to incomplete clinical information. Consequently, the final study population comprised 34 PD patients and 27 HCs.

The PD patients were further stratified into two subgroups: those with sleep disturbances (PD-SD, n = 12) and those without sleep disturbances (PD-NSD, n = 22), based on predefined objective sleep-disorder criteria derived from PSG data. This classification methodology was adapted from previous studies on PD-related sleep disorders, which utilized diagnostic frameworks based on the International Classification of Sleep Disorders in conjunction with PSG-derived objective sleep parameters. In the current study, subgroup classification was determined using available PSG measures rather than relying on questionnaire-based sleep scales. Patients who satisfied one or more PSG-based criteria were categorized as PD-SD, whereas those who did not meet these criteria were categorized as PD-NSD. The participant flowchart is shown in Fig. 1.

PD was diagnosed by experienced movement-disorder neurologists according to established clinical diagnostic criteria. Inclusion criteria for patients with PD were: (1) diagnosis of idiopathic PD; (2) early-

stage disease; (3) ability to complete MRI and overnight PSG examinations during hospitalization; (4) availability of complete clinical, PSG, and imaging data required for the present analysis; and (5) absence of severe cognitive impairment or psychiatric symptoms that could interfere with clinical assessment. Healthy controls had no history of neurological disease, no clinically significant sleep complaints, and no structural abnormalities on conventional MRI. Exclusion criteria for all participants included stroke, brain tumor, traumatic brain injury, encephalitis, atypical parkinsonism, major psychiatric disorders, MRI contraindications, significant structural brain lesions, severe imaging artifacts, excessive head motion, or incomplete clinical, sleep, or imaging data.

2.2 Clinical and polysomnographic assessment

Demographic and clinical information was collected for all participants, including age, sex, education, disease duration, medication use, and medical history. In patients with PD, motor severity was assessed using the Unified Parkinson's Disease Rating Scale Part III (UPDRS-III), and disease stage was evaluated using the Hoehn–Yahr scale. Global cognitive function was assessed using the Montreal Cognitive Assessment (MoCA) and Mini-Mental State Examination (MMSE).

Due to the potential influence of dopaminergic and sleep-related medications on sleep architecture in PD, the medication status of all patients was reviewed during hospitalization when such information was available. Patients underwent PSG and MRI while maintaining a clinically stable medication regimen, without any acute withdrawal or adjustment of antiparkinsonian medications specifically for the study. Antiparkinsonian medications were administered according to each patient's routine clinical schedule at standardized ward medication times. PSG and MRI examinations were conducted within a standardized inpatient assessment period, with MRI scans acquired during a fixed daytime scanning window to minimize variability associated with acute medication timing and circadian effects. The effects of medications were taken into account when interpreting the findings.

All patients with PD underwent overnight PSG during hospitalization. PSG was conducted to objectively assess sleep architecture, sleep continuity, and respiratory events. Sleep staging, arousals, and respiratory events were scored according to standard international criteria. PSG-derived measures included total sleep time, sleep efficiency, sleep onset latency, REM sleep latency, percentages of N1, N2, N3, and REM sleep, arousal index, and apnea–hypopnea index (AHI).

Patients were classified as PD-SD if they met one or more predefined PSG-based objective sleep-disorder criteria. These criteria included sleep onset latency > 30 minutes, indicating difficulty initiating sleep, and AHI > 5 events/hour, indicating sleep-disordered breathing. Patients who did not meet either criterion were classified as PD-NSD.

In addition to the PSG-based subgroup classification, PSG-derived sleep parameters were analyzed as continuous variables to characterize sleep architecture and to examine their associations with brainstem imaging markers and DTI-ALPS. This approach allowed us to evaluate both the presence of objectively defined sleep disturbance and the relationships between specific sleep-architecture components and

multimodal MRI measures. Because sleep-disorder classification in the present study relied on PSG-derived objective measures rather than complete questionnaire-based criteria, the PD-SD group should be interpreted as a PSG-defined sleep-disturbance group, mainly reflecting difficulty initiating sleep and/or sleep-disordered breathing.

2.3 MRI acquisition

All participants underwent MRI on a 3.0-T scanner (Philips Ingenia CX, Philips Healthcare) using a standardized protocol that included 3D T1-weighted imaging, multi-echo gradient-echo imaging for QSM reconstruction, neuromelanin-sensitive MRI, and diffusion tensor imaging. Detailed acquisition parameters for each sequence, including repetition time, echo time, flip angle, voxel size, field of view, number of diffusion directions, b values, and acquisition time, are provided in the Supplementary Methods. The overall image-processing workflow, including susceptibility reconstruction, APART-QSM source separation, NM-MRI processing, and DTI-ALPS calculation, is illustrated in Fig. 2.

2.4 Data Processing

To investigate brainstem pathology potentially involved in sleep-architecture disturbance in PD, multimodal imaging analyses focused on two neuromelanin-containing nuclei that are highly vulnerable in PD and implicated in sleep–wake regulation: the SN and LC.

2.4.1 Sub-voxel QSM analysis

QSM reconstruction was performed from multi-echo gradient-echo magnitude and phase images. Brain masks were generated from magnitude images. Phase unwrapping, background field removal, and susceptibility reconstruction were performed using established QSM processing procedures[22], including Laplacian phase unwrapping, VSHARP-based background field removal, and STAR-QSM reconstruction.

To further separate susceptibility sources, APART-QSM was applied to generate paramagnetic susceptibility maps (χ_{para}) and diamagnetic susceptibility maps (χ_{dia}). The χ_{para} map was used as an iron-related susceptibility marker. The χ_{dia} map was analyzed as as an absolute-value map; therefore, higher $|\chi_{dia}|$ values indicate increased diamagnetic susceptibility components.

All susceptibility maps were spatially normalized to MNI space through individual T1-weighted images. Briefly, susceptibility maps were co-registered to individual T1-weighted images and then transformed to MNI space using the deformation fields derived from T1-based normalization. Scalar susceptibility maps were resampled using continuous interpolation, whereas ROI masks were resampled using nearest-neighbor interpolation. For voxel-wise analyses, normalized susceptibility maps were smoothed using the Gaussian kernel and analyzed in standard space. For ROI-based analyses, unsmoothed normalized maps were used to reduce smoothing-related partial-volume effects.

Mean QSM, χ_{para}, and $|\chi_{dia}|$ values were extracted from predefined bilateral masks of the SNpc, substantia nigra pars reticulata (SNpr), and LC. ROI placement and registration accuracy were visually inspected for all participants. The susceptibility values were expressed in parts per million according to the susceptibility scaling used during QSM reconstruction.

2.4.2 Neuromelanin-sensitive MRI analysis

NM-MRI images were visually inspected for motion artifacts and image quality. SNpc regions were manually delineated on NM-MRI images in native space by trained raters with reference to anatomical landmarks. LC signal was extracted using a previously described LC mask-based approach[23]. The LC mask was transformed into each participant's native space, and mask placement was visually checked to minimize contamination from adjacent cerebrospinal fluid or pontine structures.

Neuromelanin-related signal intensity was quantified using a neuromelanin-sensitive contrast ratio, referred to as the NMratio. For both SNpc and LC measurements, the mean signal intensity of the bilateral cerebral peduncles was used as the reference signal[24]. The NMratio was calculated as:

$$NMratio = \frac{SI_{ROI} - SI_{ref}}{SI_{ref}}$$

where SI_{ROI} represents the mean signal intensity within the target ROI and SI_{ref} represents the mean signal intensity of the corresponding reference region.

Specifically, SNpc and LC contrast ratios were calculated as:

$$NMratio_{SNpc} = \frac{SI_{SNpc} - SI_{CP}}{SI_{CP}}$$

$$NMratio_{LC} = \frac{SI_{LC} - SI_{CP}}{SI_{CP}}$$

where SI_{SNpc} the mean signal intensity within the SNpc ROI, SI_{LC} represents the mean signal intensity within the LC ROI, and SI_{CP} represents the mean signal intensity of the bilateral cerebral peduncle reference regions. The primary NM-MRI metrics included bilateral SNpc NMratio and bilateral LC NMratio.

2.4.3 Glymphatic-related diffusion analysis

To explore whether sleep-related alterations in brain clearance-related processes were associated with brainstem imaging markers, glymphatic-related diffusion was assessed using the DTI-ALPS index.

DTI preprocessing included correction for head motion and eddy-current distortion, brain extraction, and diffusion tensor fitting. Directional diffusivity maps, including Dxx, Dyy, and Dzz, were generated in a standard anatomical orientation. Because reverse phase-encoding diffusion images were not available,

explicit susceptibility distortion correction was not performed. All preprocessed diffusion images and derived diffusivity maps were visually inspected for registration accuracy and gross artifacts.

The DTI-ALPS index was calculated according to the method proposed by Yokota et al. Briefly[21], template-based ROIs were placed in projection-fiber and association-fiber regions at the level of the lateral ventricular body in standard space and then applied to the corresponding directional diffusivity maps. ROI placement was not manually drawn for each participant; instead, standard-space ROIs were used and visually checked to confirm appropriate anatomical positioning after spatial normalization. Directional diffusivities were extracted from each ROI, and the ALPS index was calculated as:

$$\mathrm{DTI-ALPS} = \frac{\mathrm{mean}(Dxx_{proj},\ Dxx_{assoc})}{\mathrm{mean}(Dyy_{proj},\ Dzz_{assoc})}$$

where $Dxx_{proj}$and Dxx_{assoc}represent diffusivity along the right–left direction in projection-fiber and association-fiber regions, respectively; Dyy_{proj}represents diffusivity along the anterior–posterior direction in projection-fiber regions; and Dzz_{assoc}represents diffusivity along the inferior–superior direction in association-fiber regions. Higher ALPS values were interpreted as reflecting greater diffusivity along the perivascular-space direction and potentially more preserved glymphatic-related diffusion[25]. Left and right ALPS values were averaged for subsequent analyses; hemisphere-specific ALPS analyses were not performed.

2.5 Statistical analysis

Statistical analyses were performed using SPSS 25.0, R version 4.3.0, and SPM12. Continuous variables were inspected for normality using the Shapiro–Wilk test and visual assessment of histograms. Normally distributed variables are presented as mean ± standard deviation, whereas non-normally distributed variables are presented as median and interquartile range when appropriate. Categorical variables are presented as counts and percentages.

Demographic and clinical variables were compared among groups using one-way analysis of variance or the Kruskal–Wallis test for continuous variables, as appropriate. Categorical variables were compared using the chi-square test or Fisher’s exact test. For comparisons restricted to patients with PD, including disease duration, Hoehn–Yahr stage, UPDRS-III scores, and PSG-derived sleep parameters, independent-sample t tests or Mann–Whitney U tests were used as appropriate.

ROI-based imaging analyses were performed to compare susceptibility-derived and neuromelanin-sensitive MRI metrics among groups. For PD versus HC comparisons, analysis of covariance was used with age and sex included as covariates. For three-group comparisons among PD-SD, PD-NSD, and HCs, analysis of covariance was also performed with age and sex as covariates, followed by post-hoc pairwise comparisons when the overall group effect was significant. Given the modest sample size and exploratory nature of the ROI-based analyses, two-sided raw P values are reported unless otherwise specified, and these findings were interpreted as exploratory.

Voxel-wise analyses of QSM, χ_{para}, and $|\chi_{dia}|$ maps were performed in FSL using general linear models, with age and sex included as nuisance covariates. Smoothed normalized susceptibility maps were used for voxel-wise analyses. Statistical significance was determined using family-wise error correction, with $P_{FWE} < 0.05$ considered significant. Small-volume correction was not applied unless otherwise specified.

Associations among imaging markers, PSG-derived sleep parameters, and DTI-ALPS indices were assessed using exploratory partial correlation analyses controlling for age and sex. These correlation analyses were conducted to examine relationships among brainstem susceptibility alterations, neuromelanin-sensitive signal, sleep architecture, and glymphatic-related diffusion. Given the exploratory design and modest sample size, raw P values are reported for correlation analyses, and results were interpreted cautiously.

Receiver operating characteristic (ROC) analyses were performed to evaluate the apparent discriminative performance of individual imaging markers and combined multimodal imaging models. The area under the curve, sensitivity, specificity, and accuracy were calculated for each model. For combined models, candidate imaging markers showing exploratory group differences in ROI-based analyses were entered into multivariable logistic regression models, and predicted probabilities were used to construct ROC curves. Given the modest sample size, the combined models were intended for exploratory assessment only and were not used to establish diagnostic thresholds. Because the sample size was modest, particularly in the PD-SD subgroup, and no independent validation or cross-validation was performed, ROC results were considered exploratory and are reported as apparent discriminative performance rather than validated diagnostic accuracy. Statistical significance was set at a two-tailed $P < 0.05$.

3. Results

3.1 Demographic and polysomnographic characteristics

The demographic, clinical, and polysomnographic characteristics of the study cohort are detailed in Table 1. The distribution of age and sex did not exhibit significant differences among the PD-SD, PD-NSD, and HC groups. Within the PD cohort, disease duration, H-Y stage, and UPDRS-III scores were comparable between the PD-SD and PD-NSD subgroups.

Table 1
Demographic and clinical characteristics of the participants.

Age (years)	**PD-SD**	**PD-NSD**	**HC**	**P value**
	64.4 ± 8.5	**60.68 ± 10.1**	**59.7 ± 6.1**	**0.083†**
Sex (M/F)	6/6	10/12	10/17	0.710‡
Disease duration (years)	5.75 ± 3.5	5.63 ± 2.2	NA	0.902
H-Y stage	2.54 ± 0.9	2.27 ± 0.9	NA	0.091
UPDRS-III	35.00 ± 23.0	39.27 ± 18.3	NA	0.557
Total sleep time (minutes)	304.00 ± 126.41	324.43 ± 113.3	NA	0.633
Sleep efficiency	54.93 ± 18.1	62.51 ± 17.7	NA	0.245
Arousal count	147.75 ± 61.4	63.45 ± 47.3	NA	< 0.001*
AI	69.69 ± 136.6	12.21 ± 4.9	NA	0.054
REM	21.08 ± 15.6	49.68 ± 28.3	NA	0.003*
REM%	0.07 ± 0.04	0.15 ± 0.08	NA	0.003*
N1	109.00 ± 56.2	65.89 ± 35.1	NA	0.010*
N2	128.00 ± 58.8	170.89 ± 80.9	NA	0.116
N3	31.92 ± 29.4	37.98 ± 36.5	NA	0.625
N3%	0.10 ± 0.09	0.12 ± 0.10	NA	0.585
AHI	13.75 ± 15.7	2.81 ± 2.9	NA	0.035*

Note. Continuous variables are expressed as mean ± SD; † one-way ANOVA analysis; ‡ Chi-square test; *P < 0.05. AI: arousal index; REM: rapid eye movement; AHI: apnea-hypopnea index; H-Y: Hoehn and Yahr; PD-SD: Parkinson's disease with sleep disturbance, PD-NSD: Parkinson's disease without sleep disturbance; HC: healthy controls.

According to predefined PSG-derived objective criteria, 12 patients were classified as PD-SD, while 22 were classified as PD-NSD. In this study, the PD-SD subgroup represented a PSG-defined sleep disturbance phenotype, primarily characterized by difficulties in sleep initiation and/or sleep-disordered breathing. Consequently, PSG parameters employed for subgroup classification, such as sleep onset latency and the AHI, were regarded as defining characteristics of the phenotype rather than independent outcomes. Beyond these defining parameters, the PD-SD group exhibited a reduced proportion of REM sleep and prolonged N1 sleep duration compared to the PD-NSD group, indicating altered sleep-stage organization in patients with PSG-defined sleep disturbances.

3.2 Brainstem imaging profiles associated with PSG-defined sleep disturbance in PD

To investigate whether PSG-defined sleep-architecture phenotypes in PD were associated with MRI-derived abnormalities of brainstem nuclei involved in sleep-wake regulation, we examined susceptibility-derived and neuromelanin-sensitive MRI metrics in the SN and LC.

Voxel-wise analysis of the signed diamagnetic susceptibility map revealed a significant group difference in the substantia nigra (Fig. 3 and Table 2). Compared with the PD-SD group, the PD-NSD group showed significantly higher $|\chi_{dia}|$ values in a substantia nigra cluster (273 voxels; $P_{FWE} = 0.042$; peak MNI coordinates: x = 13, y = − 18, z = − 16). This cluster included 114 voxels within the SNpc and 159 voxels within the SNpr. ROI-based analyses further demonstrated distinct LC–SN imaging profiles across groups (Fig. 4 and Table 3). Compared with HCs, patients with PD showed higher χ_{para} in the right SNpc, lower χ_{para} in the right LC, and reduced NM ratio in the bilateral SNpc.

Table 2
Significant cluster of magnetic susceptibility in SN and LC among groups.

Brain regions	**Cluster size (voxels)**	**P_{FWE} value**	**Peak MNI coordinate (mm)**		
			X	**Y**	**Z**
χ_{dia}					
PD-NSD > PD-SD	273	0.042	13	-18	-16
SNpc_L	114				
SNpr_L	159				

Note. MNI: Montreal Neurological Institute; P_{FWE}: familywise error corrected p-value; χ_{dia}: diamagnetic susceptibility mapping; PD-SD: Parkinson's disease with sleep disturbance, PD-NSD: Parkinson's disease without sleep disturbance; SN: substantia nigra; LC: locus coeruleus; SNpc_L: left substantia nigra (pars compacta); SNpr_L: left substantia nigra (pars reticulata).

Table 3
Significant ROIs of magnetic susceptibility in SN and LC among groups.

ROIs	PD	HC	P value (PD vs. HC)	PD-NSD	PD-SD	P value (ANOVA)	P value (post-hoc)		
							PD-SD vs. HC	PD-NSD vs. HC	PD-SD vs. PD-NSD
$\lvert\chi_{dia}\rvert$ (ppm)									
SNpc_L	0.020 ± 0.007	0.017 ± 0.006	0.036	0.022 ± 0.006	0.017 ± 0.006	0.036	0.756	0.004	0.040
χ_{para} (ppm)									
LC_R	0.005 ± 0.004	0.008 ± 0.005	0.027	0.005 ± 0.005	0.004 ± 0.002	0.014	0.008	0.054	0.292
SNpc_R	0.085 ± 0.029	0.068 ± 0.024	0.047	0.083 ± 0.030	0.089 ± 0.028	0.052	NA	NA	NA
NMratio									
SNpc_L	0.075 ± 0.043	0.105 ± 0.032	0.022	0.081 ± 0.042	0.065 ± 0.045	0.022	0.004	0.029	0.262
SNpc_R	0.067 ± 0.042	0.099 ± 0.034	0.008	0.075 ± 0.038	0.052 ± 0.045	0.008	0.029	0.001	0.095

Note. PD-SD: Parkinson's disease with sleep disturbance, PD-NSD: Parkinson's disease without sleep disturbance; HC: healthy controls; χ_{dia}: diamagnetic susceptibility mapping; χ_{para}: paramagnetic susceptibility mapping; SN: substantia nigra; LC: locus coeruleus; SNpc_L: left substantia nigra (pars compacta); SNpc_R: right substantia nigra (pars compacta); LC_R: right locus coeruleus. P values are uncorrected two-sided values from exploratory analyses.

When patients with PD were stratified according to PSG-defined sleep-architecture phenotype, significant group effects were observed for $\lvert\chi_{dia}\rvert$ of SNpc, χ_{para} of right LC, and NMratio in the bilateral SNpc. The PD-NSD group showed higher $\lvert\chi_{dia}\rvert$ value of SNpc than that in both the PD-SD and HC groups. The χ_{para} of right LC was significantly lower in the PD-SD group than in HCs, whereas the difference between PD-SD and PD-NSD did not reach statistical significance. The NMratio in bilateral SNpc was lower in patients with PD than in HCs, with numerically lower values in the PD-SD group than in the PD-NSD group; however, the direct comparison between PD-SD and PD-NSD was not statistically significant.

3.3 Associations between brainstem imaging markers and sleep architecture

To determine whether LC–SN imaging markers were related to objective sleep structure, exploratory partial correlation analyses were performed between imaging metrics and PSG-derived sleep parameters, with age and sex controlled as covariates. Within the PD cohort, χ_{para} in the right LC was positively correlated with N3 sleep percentage (r = 0.38, P = 0.030; Fig. 5B). In addition, $|\chi_{dia}|$ of SNpc was positively associated with REM sleep percentage (r = 0.36, P = 0.045; Fig. 5B).

3.4 Glymphatic-related diffusion and sleep architecture

Given the established relationship between sleep and brain clearance-related processes, we next examined whether glymphatic-related diffusion, measured by DTI-ALPS, was associated with sleep architecture and brainstem imaging markers. A higher DTI-ALPS index was significantly associated with a higher proportion of N3 sleep (r = 0.43, P = 0.022; Fig. 5C), suggesting that glymphatic-related diffusion may be linked to slow-wave sleep in patients with PD. Furthermore, the DTI-ALPS index was positively correlated with χ_{para} in the right LC (r = 0.45, P = 0.016; Fig. 5C).

3.5 Coupling between iron-related susceptibility and neuromelanin signal

Across all participants, NMratio in the left SNpc was negatively correlated with χ_{para} value of right SNpc (r = − 0.39, P = 0.002; Fig. 5A). Similarly, NMratio in the right SNpc was negatively correlated with χ_{para} of right SNpc (r = − 0.38, P = 0.003; Fig. 5A).

3.6 Diagnostic performance of multimodal imaging markers

Results of ROC were shown in Fig. 6. For discriminating patients with PD from HCs, the combined multimodal model achieved an AUC of 0.82, with a sensitivity of 79.4%, specificity of 81.5%, and accuracy of 80.3% (Fig. 6A). For discriminating PD-SD from HCs, the combined model showed an AUC of 0.89, with a sensitivity of 91.7%, specificity of 85.2%, and accuracy of 87.2% (Fig. 6B). For discriminating PD-NSD from HCs, the corresponding AUC was 0.81, with a sensitivity of 77.3%, specificity of 74.1%, and accuracy of 75.5% (Fig. 6C). Overall, multimodal models combining susceptibility-derived and neuromelanin-sensitive MRI metrics showed higher apparent discriminative performance than individual imaging markers.

4. Discussion

In this multimodal MRI study, which integrates polysomnography, APART-QSM, neuromelanin-sensitive MRI, and DTI-ALPS, we explored the associations among PSG-defined sleep disturbances, LC–SN

imaging markers, and glymphatic-related diffusion in individuals with early-stage Parkinson's disease. The principal findings are as follows: Firstly, patients with PD-SD exhibited distinct LC–SN imaging profiles compared to those with PD-NSD and HCs. This included a lower right LC χ_{para} relative to HCs, altered $|\chi_{dia}|$ of SN, and a reduced NMratio in the SNpc in PD. Secondly, LC and SN imaging markers were correlated with specific components of objective sleep architecture, notably N3 and REM sleep. Thirdly, DTI-ALPS was associated with both the percentage of N3 sleep and LC susceptibility measures. Lastly, SNpc paramagnetic susceptibility demonstrated an inverse relationship with the neuromelanin-sensitive signal in the SNpc. Collectively, these findings imply a potential interrelationship among brainstem imaging abnormalities, sleep architecture, and glymphatic-related diffusion in Parkinson's disease.

4.1 Distinct LC–SN imaging profiles are associated with PSG-defined sleep disturbance in PD

Sleep disturbances are among the most prevalent and clinically significant non-motor symptoms of PD. In the current cohort, PD-SD were characterized using objective PSG criteria, primarily indicating difficulties in sleep initiation and/or sleep-disordered breathing. Beyond these defining characteristics, patients with PD-SD also exhibited altered sleep-stage organization, including a reduced proportion of REM sleep and prolonged N1 sleep duration. These observations align with the understanding that sleep disturbances in PD are heterogeneous, potentially involving disruptions in both sleep continuity and sleep-stage organization.

Notably, PSG-defined sleep disturbances were correlated with distinct imaging profiles of the LC–SN. Compared to HCs, PD patients demonstrated a reduced NMratio in the bilateral SNpc, indicating a loss of neuromelanin neuro within the SNpc. Furthermore, patients with PD-SD exhibited lower χ_{para} values in the right LC than in HCs, indicating reduced iron content in the LC. PD-NSD showed a higher $|\chi_{dia}|$ value of SNpc than that in both PD-SD patients and HCs, which may imply the aggregation of diamagnetic susceptibility components, including α-synuclein, calcium, and plastic myelination. These findings should not be construed as indicative of a straightforward linear pattern of more severe brainstem degeneration in PD-SD. Rather, they suggest that different PSG-defined sleep phenotypes in PD may be associated with different sub-voxel susceptibility and neuromelanin-sensitive imaging patterns within the LC–SN system.

The interpretation of LC sub-voxel susceptibility changes requires careful consideration. In contrast to χ_{para} in the SN, which is frequently regarded as an indicator of iron-related susceptibility, LC susceptibility is potentially influenced by a variety of tissue characteristics, including neuromelanin content, iron binding, local microstructure, and partial-volume effects[23]. Consequently, the observed reduction in χ_{para} in the LC in individuals with PD-SD compared to HCs may indicate susceptibility alterations within a sleep–wake regulatory nucleus that is vulnerable, but it should not be construed as a direct measure of iron loss or gain. These findings underscore the involvement of neuromelanin-containing brainstem nuclei in sleep disturbances associated with Parkinson's disease, while also emphasizing the necessity

for larger-scale studies that incorporate more detailed sleep phenotyping and histopathological or molecular validation.

4.2 LC and SN imaging abnormalities are associated with objective sleep architecture

A significant strength of this study lies in the integration of multimodal brainstem imaging with objective polysomnographic measurements. Instead of relying solely on subjective sleep complaints or questionnaire-based assessments, we investigated the relationships between imaging markers and specific components of sleep architecture.

Within the PD cohort, LC sub-voxel QSM was associated with the percentage of N3 sleep, while SN diamagnetic susceptibility was linked to the percentage of REM sleep. Although these associations should be interpreted with caution, they indicate that different components of brainstem pathology may contribute to distinct aspects of sleep regulation.

The LC is pivotal in arousal regulation and REM sleep modulation through its extensive noradrenergic projections[26]. Previous experimental and clinical studies have implicated LC degeneration in various non-motor manifestations of PD, including sleep dysfunction[27]. Therefore, the observed association between LC susceptibility and N3 sleep supports a potential link between alterations in LC susceptibility and objective sleep architecture.

Similarly, although the SN is traditionally viewed in relation to motor dysfunction, dopaminergic pathways also participate in arousal regulation, sleep maintenance, and REM sleep organization[28]. Experimental and clinical studies have shown that dopaminergic dysfunction alters sleep–wake transitions and REM sleep expression[29]. Consequently, abnormalities within both the LC and SN may contribute to sleep disturbances through partially overlapping yet distinct neurophysiological mechanisms.

Taken together, these findings suggest that objective sleep-architecture abnormalities in PD may be associated with alterations in interconnected brainstem networks involved in sleep regulation, although causality cannot be inferred from the present cross-sectional data.

4.3 Glymphatic-related diffusion is associated with sleep architecture and LC susceptibility

A significant finding of the current study is the association between glymphatic-related diffusion, as assessed via DTI-ALPS, and both the percentage of N3 sleep and LC susceptibility measures in patients with PD. Although DTI-ALPS does not directly quantify glymphatic flow, it serves as an indirect MRI marker for perivascular-space-related diffusivity and has been employed to characterize brain clearance-related diffusion in neurodegenerative disorders.

Sleep is hypothesized to play a crucial role in sustaining brain clearance processes. Experimental and clinical research indicates that slow-wave sleep may enhance cerebrospinal fluid–interstitial fluid

exchange and facilitate the removal of metabolic waste products, whereas sleep fragmentation and disrupted sleep continuity may negatively impact these processes[30]. Consistent with this framework, we identified a positive correlation between DTI-ALPS and the percentage of N3 sleep, suggesting that preserved slow-wave sleep may be associated with more favorable perivascular diffusion characteristics in PD.

Additionally, DTI-ALPS was positively correlated with χ_{para} in the right LC. The LC is a critical nucleus involved in the regulation of arousal, sleep–wake transitions, and autonomic modulation. Therefore, the association between LC sub-voxel QSM and DTI-ALPS raises the possibility that alterations within sleep-regulating brainstem nuclei may be related not only to sleep architecture but also to downstream perivascular diffusion characteristics. However, sub-voxel QSM in the LC is an indirect imaging measure and may be influenced by neuromelanin, iron binding, local tissue microstructure, and partial-volume effects. Therefore, this association should be interpreted cautiously and should not be taken as direct evidence of LC pathology or glymphatic dysfunction.

It should also be noted that AHI was one of the PSG-based criteria used to define PD-SD in the present study. Therefore, the higher apnea–hypopnea burden in the PD-SD group should be interpreted as a defining component of the PSG-defined sleep-disturbance phenotype rather than as an independent finding. Sleep-disordered breathing may contribute to sleep fragmentation, altered sleep-stage organization, intermittent hypoxia, and changes in perivascular diffusion characteristics[31]. Thus, the present PD-SD classification should be interpreted as an objective PSG-defined sleep-disturbance phenotype mainly reflecting difficulty initiating sleep and/or sleep-disordered breathing, rather than a disorder-specific category such as RBD, insomnia, or restless legs syndrome.

Taken together, these findings suggest a potential link among slow-wave sleep, LC sub-voxel QSM, and glymphatic-related diffusion in PD. Because of the cross-sectional design, causality cannot be inferred. Future studies should separately model sleep onset difficulty, sleep-disordered breathing, REM sleep abnormalities, and other sleep-disorder subtypes to determine whether LC–SN imaging alterations and DTI-ALPS changes are specific to particular sleep phenotypes in PD.

4.4 Interrelationship among brainstem imaging markers, sleep architecture, and glymphatic-related diffusion in PD

Instead of pinpointing a singular imaging biomarker for PD-related sleep disturbances, this study proposes a comprehensive framework wherein alterations in LC–SN imaging, objective sleep architecture abnormalities, and glymphatic-related diffusion are interrelated components of PD pathophysiology.

Beyond the associations between sleep architecture and DTI-ALPS, we identified a negative correlation between χ_{para} and NMratio in the SNpc. This observation aligns with the hypothesis that changes in iron-related susceptibility and neuromelanin-sensitive signal loss may reflect complementary vulnerabilities within catecholaminergic neurons. Neuromelanin has the capacity to bind metal ions, and the

degeneration of neuromelanin-containing neurons may disrupt local iron homeostasis, thereby increasing neuronal vulnerability[32]. Nonetheless, NM-MRI and susceptibility-derived metrics are indirect imaging markers and should not be construed as direct histopathological indicators.

Collectively, our findings endorse a hypothesis-generating model suggesting that alterations in neuromelanin-containing brainstem nuclei are linked to sleep architecture abnormalities, changes in sleep physiology may be indicative of glymphatic-related diffusion. These processes may interact during PD progression, but the present cross-sectional data do not establish temporal sequence or causality. Longitudinal studies integrating repeated PSG, multimodal MRI, and molecular biomarkers are needed to determine whether LC–SN imaging abnormalities predict the development or progression of sleep disturbance in PD.

4.5 Limitations and future directions

Several limitations should be acknowledged. First, the sample size was modest, particularly within the PD-SD subgroup, which may have limited statistical power and reduced the stability of subgroup and correlation analyses. Second, the cross-sectional design precludes determination of temporal or causal relationships among LC–SN imaging alterations, sleep disturbance, and glymphatic-related diffusion. Third, PD-SD was defined using available PSG-based objective criteria, mainly reflecting difficulty initiating sleep and/or sleep-disordered breathing. Although this approach provided an objective sleep-disturbance classification, it did not allow detailed separation of specific sleep-disorder subtypes such as RBD, insomnia, restless legs syndrome, or periodic limb movements. In addition, AHI was one of the criteria used for subgroup classification; therefore, the contribution of sleep-disordered breathing to the observed imaging and DTI-ALPS findings should be considered. Fourth, although PSG and MRI were performed during hospitalization under a clinically stable medication regimen and with standardized medication and examination timing as far as possible, detailed levodopa-equivalent daily dose was not calculated and could not be included as a covariate. Finally, APART-QSM, NM-MRI, and DTI-ALPS are indirect imaging markers, and accurate assessment of the LC and SN remains technically challenging because of their small size and susceptibility to partial-volume effects. Future longitudinal studies with larger samples, detailed medication quantification, formal sleep-disorder phenotyping, and repeated multimodal MRI and PSG assessments are needed to validate and extend these findings.

5. Conclusions

In conclusion, this multimodal MRI study indicates that sleep disturbances associated with PD are linked to a comprehensive brainstem-centered imaging profile, specifically involving the LC and SN. The study identified alterations in LC susceptibility, a reduction in neuromelanin-sensitive signals in the SNpc, and changes in the diamagnetic susceptibility of the SN across various PD sleep phenotypes. These brainstem imaging markers were correlated with objective measures of sleep architecture, while glymphatic-related diffusion was associated with both slow-wave sleep and LC susceptibility metrics. The findings propose a hypothesis-generating framework involving the LC, SN, sleep, and glymphatic-related diffusion in PD, suggesting that imaging alterations in vulnerable neuromelanin-containing

brainstem nuclei, disrupted sleep architecture, and modified clearance-related diffusion may constitute interconnected elements of the disease's pathophysiology. Given the cross-sectional nature of the current study, these associations should be considered hypothesis-generating. Future longitudinal research incorporating multimodal MRI, molecular biomarkers, and repeated polysomnographic assessments is necessary to ascertain whether LC–SN imaging abnormalities can serve as early indicators of PD sleep phenotypes and disease progression.

Declarations

Data/code availability

The materials and code used and/or analyzed during the current study are available from the corresponding author upon reasonable request after the entire data collection procedure and project are completed.

Ethics statement

This study was approved by the Ethics Committee of Shandong Provincial Hospital. All procedures involving human participants followed institutional guidelines and the principles of the Declaration of Helsinki. Written informed consent was obtained from all participants or their legally authorized representatives before participation.

Funding

This work was supported by the Natural Science Foundation of Shandong Province (Grant Nos. ZR2026QC1728).

Contributions

(I) Conception and design: Aocai Yang; (II) Administrative support: Guangbin Wang and Yuanyuan Xiang; (III) Provision of study materials or patients: All authors; (IV) Collection and assembly of data: Yuxin Li; (V) Data analysis and interpretation: Aocai Yang and Yuxin Li; (VI) Manuscript writing: Aocai Yang and Yuxin Li; (VII) Final approval of manuscript: All authors.

Declaration of Competing Interest

The authors declare that they have no conflict of interest.

Acknowledgements

The authors thank all participants in the study.

References

1. SVEINBJORNSDOTTIR S. The clinical symptoms of Parkinson's disease[J/OL]. Journal of Neurochemistry, 2016, 139(S1): 318–324. DOI:10.1111/jnc.13691.
2. CHAUDHURI K R, HEALY D G, SCHAPIRA A H. Non-motor symptoms of Parkinson's disease: diagnosis and management[J/OL]. The Lancet Neurology, 2006, 5(3): 235–245. DOI:10.1016/S1474-4422(06)70373-8.
3. ARNULF I. Excessive daytime sleepiness in parkinsonism[J/OL]. Sleep Medicine Reviews, 2005, 9(3): 185–200. DOI:10.1016/j.smrv.2005.01.001.
4. IRANZO A, FERNÁNDEZ-ARCOS A, TOLOSA E, et al. Neurodegenerative Disorder Risk in Idiopathic REM Sleep Behavior Disorder: Study in 174 Patients[J/OL]. PLoS ONE, 2014, 9(2): e89741. DOI:10.1371/journal.pone.0089741.
5. RAZQUIN J, DE LAS HERAS-GARCÍA L, VAQUERO-RODRÍGUEZ A, et al. Locus coeruleus α-synuclein overexpression induces prodromal Parkinsonian features in mice[J/OL]. npj Parkinson's Disease, 2026[2026-06-27]. https://www.nature.com/articles/s41531-026-01420-w. DOI:10.1038/s41531-026-01420-w.
6. PASQUINI J, FIRBANK M J, BEST L, et al. Substantia nigra and locus coeruleus microstructural abnormalities in isolated rapid eye movement sleep behaviour disorder and Parkinson's disease[J/OL]. Brain Communications, 2025, 7(1): fcaf023. DOI:10.1093/braincomms/fcaf023.
7. YADAV R K, KHANDAY M A, MALLICK B N. Interplay of dopamine and GABA in substantia nigra for the regulation of rapid eye movement sleep in rats[J/OL]. Behavioural Brain Research, 2019, 376: 112169. DOI:10.1016/j.bbr.2019.112169.
8. COOKE L E, ROCHA E, DIMAIO R, et al. The irony of Parkinson's disease: Converging mechanisms of redox imbalance and ferroptosis[J/OL]. Redox Biology, 2026, 95: 104239. DOI:10.1016/j.redox.2026.104239.
9. YAO Z, JIAO Q, DU X, et al. Ferroptosis in Parkinson's disease -- The iron-related degenerative disease[J/OL]. Ageing Research Reviews, 2024, 101: 102477. DOI:10.1016/j.arr.2024.102477.
10. ZAHED H, ZUZUARREGUI J R P, GILRON R, et al. The Neurophysiology of Sleep in Parkinson's Disease[J/OL]. Movement Disorders, 2021, 36(7): 1526–1542. DOI:10.1002/mds.28562.
11. SALAZAR J, MENA N, NÚÑEZ M T. Iron dyshomeostasis in Parkinson's disease[J/OL]. Journal of Neural Transmission. Supplementum, 2006(71): 205–213. DOI:10.1007/978-3-211-33328-0_22.
12. GUAN X, LANCIONE M, AYTON S, et al. Neuroimaging of Parkinson's disease by quantitative susceptibility mapping[J/OL]. NeuroImage, 2024, 289: 120547. DOI:10.1016/j.neuroimage.2024.120547.
13. DOUBLE K L, GERLACH M, SCHÜNEMANN V, et al. Iron-binding characteristics of neuromelanin of the human substantia nigra[J/OL]. Biochemical Pharmacology, 2003, 66(3): 489–494. DOI:10.1016/s0006-2952(03)00293-4.
14. ZECCA L, CASELLA L, ALBERTINI A, et al. Neuromelanin can protect against iron-mediated oxidative damage in system modeling iron overload of brain aging and Parkinson's disease[J/OL]. Journal of Neurochemistry, 2008, 106(4): 1866–1875. DOI:10.1111/j.1471-4159.2008.05541.x.

15. WANG Y, LIU T. Quantitative susceptibility mapping (QSM): Decoding MRI data for a tissue magnetic biomarker[J/OL]. Magnetic Resonance in Medicine, 2015, 73(1): 82–101. DOI:10.1002/mrm.25358.
16. SHIN H G, LEE J, YUN Y H, et al. χ-separation: Magnetic susceptibility source separation toward iron and myelin mapping in the brain[J/OL]. NeuroImage, 2021, 240: 118371. DOI:10.1016/j.neuroimage.2021.118371.
17. LI Z, FENG R, LIU Q, et al. APART-QSM: An improved sub-voxel quantitative susceptibility mapping for susceptibility source separation using an iterative data fitting method[J/OL]. NeuroImage, 2023, 274: 120148. DOI:10.1016/j.neuroimage.2023.120148.
18. BURADE A, LAKHANI D A, DAGHER R, et al. Beyond Parkinson's Disease: A Narrative Review of Neuromelanin MRI in Neurodegenerative Diseases[J/OL]. Journal of Neuroimaging: Official Journal of the American Society of Neuroimaging, 2025, 35(6): e70113. DOI:10.1111/jon.70113.
19. URSO D, GNONI V, ROLLO E, et al. The Glymphatic System and Sleep Dysfunction in Parkinson's Disease[J/OL]. Sleep Medicine Clinics, 2025, 20(3): 379–387. DOI:10.1016/j.jsmc.2025.06.008.
20. ILIFF J J, WANG M, LIAO Y, et al. A Paravascular Pathway Facilitates CSF Flow Through the Brain Parenchyma and the Clearance of Interstitial Solutes, Including Amyloid β[J/OL]. Science Translational Medicine, 2012, 4(147)[2026-02-28]. https://www.science.org/doi/10.1126/scitranslmed.3003748. DOI:10.1126/scitranslmed.3003748.
21. WOOD K H, NENERT R, MIFTEN A M, et al. Diffusion Tensor Imaging-Along the Perivascular-Space Index Is Associated with Disease Progression in Parkinson's Disease[J/OL]. Movement Disorders: Official Journal of the Movement Disorder Society, 2024, 39(9): 1504–1513. DOI:10.1002/mds.29908.
22. DONG L, ZHOU W, AN R, . Paramagnetic susceptibility mapping better quantifies brain iron content in Parkinson's disease with RBD[J/OL]. npj Parkinson's Disease, 2025, 11(1): 192. DOI:10.1038/s41531-025-01043-7.
23. BETTS M J, CARDENAS-BLANCO A, KANOWSKI M, et al. In vivo MRI assessment of the human locus coeruleus along its rostrocaudal extent in young and older adults[J/OL]. NeuroImage, 2017, 163: 150–159. DOI:10.1016/j.neuroimage.2017.09.042.
24. LAKHANI D A, ZHOU X, TAO S, et al. Diagnostic utility of 7T neuromelanin imaging of the substantia nigra in Parkinson's disease[J/OL]. npj Parkinson's Disease, 2024, 10(1): 13. DOI:10.1038/s41531-024-00631-3.
25. TAOKA T, MASUTANI Y, KAWAI H, et al. Evaluation of glymphatic system activity with the diffusion MR technique: diffusion tensor image analysis along the perivascular space (DTI-ALPS) in Alzheimer's disease cases[J/OL]. Japanese Journal of Radiology, 2017, 35(4): 172–178. DOI:10.1007/s11604-017-0617-z.
26. TARGA A D S, RODRIGUES L S, NOSEDA A C D, et al. Unraveling a new circuitry for sleep regulation in Parkinson's disease[J/OL]. Neuropharmacology, 2016, 108: 161–171. DOI:10.1016/j.neuropharm.2016.04.018.

27. ACOSTA-CABRONERO J, BETTS M J, CARDENAS-BLANCO A, et al. In Vivo MRI Mapping of Brain Iron Deposition across the Adult Lifespan[J/OL]. The Journal of Neuroscience: The Official Journal of the Society for Neuroscience, 2016, 36(2): 364–374. DOI:10.1523/JNEUROSCI.1907-15.2016.
28. SAMIZADEH M A, FALLAH H, TOOMARISAHZABI M, et al. Parkinson's Disease: A Narrative Review on Potential Molecular Mechanisms of Sleep Disturbances, REM Behavior Disorder, and Melatonin[J/OL]. Brain Sciences, 2023, 13(6): 914. DOI:10.3390/brainsci13060914.
29. SUN J, LAI Z, MA J, et al. Quantitative evaluation of iron content in idiopathic rapid eye movement sleep behavior disorder[J/OL]. Movement Disorders: Official Journal of the Movement Disorder Society, 2020, 35(3): 478–485. DOI:10.1002/mds.27929.
30. SIOW T Y, TOH C H, HSU J L, et al. Association of Sleep, Neuropsychological Performance, and Gray Matter Volume With Glymphatic Function in Community-Dwelling Older Adults[J/OL]. Neurology, 2022, 98(8)[2026-02-28]. https://www.neurology.org/doi/10.1212/WNL.0000000000013215. DOI:10.1212/WNL.0000000000013215.
31. LIN S, LIN X, CHEN S, et al. Association of MRI Indexes of the Perivascular Space Network and Cognitive Impairment in Patients with Obstructive Sleep Apnea[J/OL]. Radiology, 2024, 311(3): e232274. DOI:10.1148/radiol.232274.
32. BAGWE-PARAB S, KAUR G. Molecular targets and therapeutic interventions for iron induced neurodegeneration[J/OL]. Brain Research Bulletin, 2020, 156: 1–9. DOI:10.1016/j.brainresbull.2019.12.011.

Figures

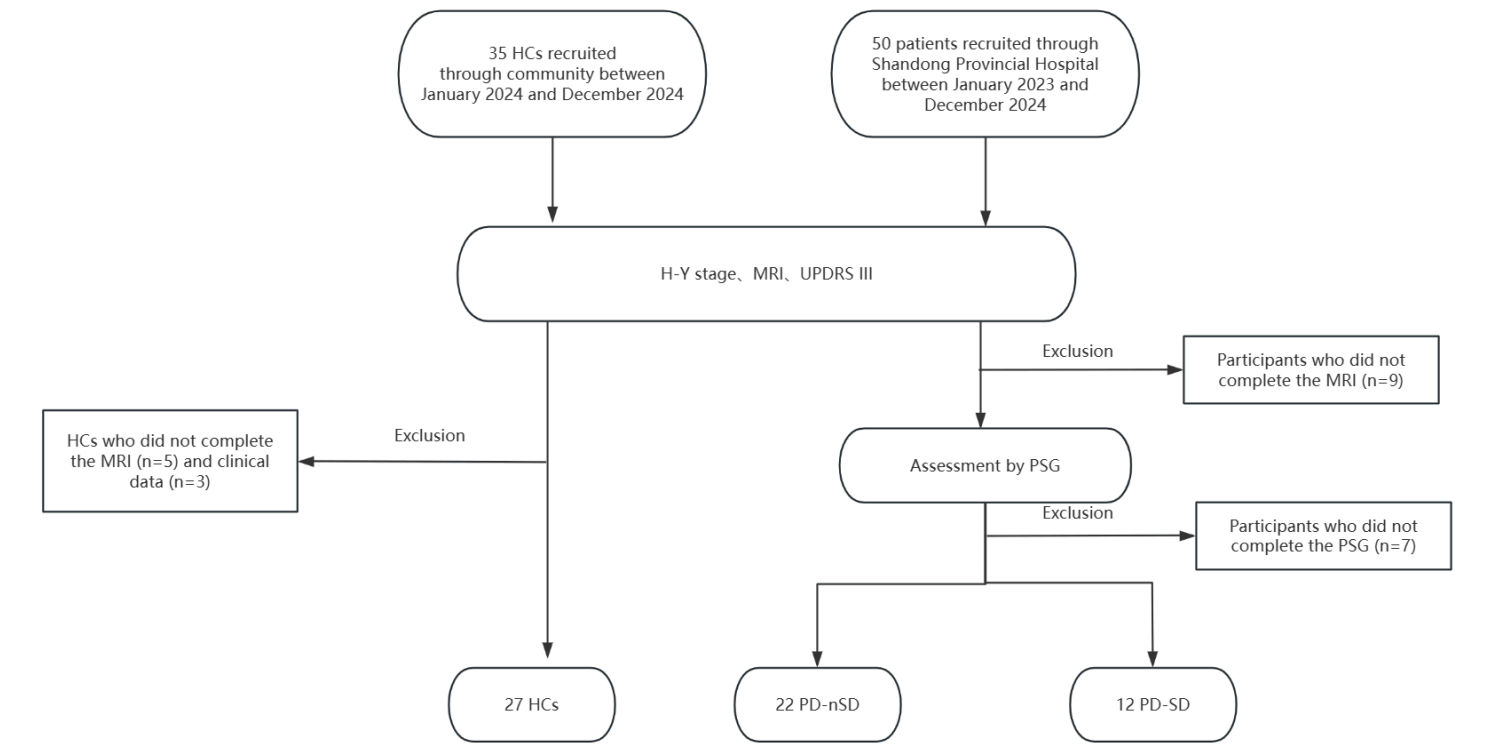


Figure 1

Participant enrollment and grouping flowchart. A total of 35 healthy controls (HCs) were recruited from the community between January 2024 and December 2024, and 50 patients with Parkinson's disease (PD) were recruited from Shandong Provincial Hospital between January 2023 and December 2024. All participants underwent clinical assessment and MRI scanning, including Hoehn and Yahr staging and Unified Parkinson's Disease Rating Scale part III (UPDRS-III) assessment. Among HCs, 5 participants who did not complete MRI and 3 participants with incomplete clinical data were excluded, leaving 27 HCs for the final analysis. Among patients with PD, 9 participants who did not complete MRI and 7 participants who did not complete polysomnography (PSG) were excluded. Based on PSG assessment, the remaining patients were classified into PD with sleep disturbance (PD-SD, n = 12) and PD without sleep disturbance (PD-NSD, n = 22) groups.

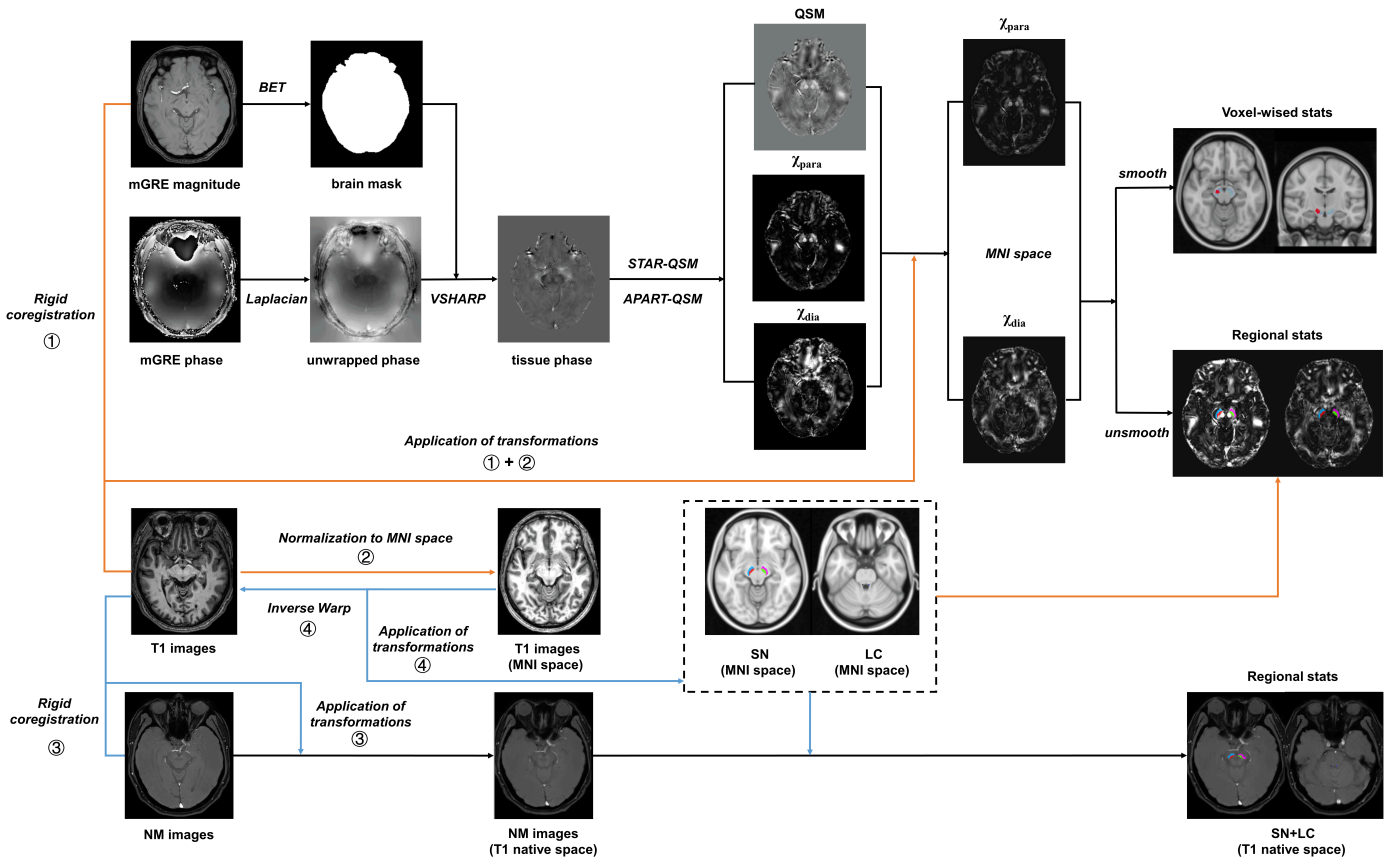


Figure 2

Multimodal MRI processing workflow. Multi-echo gradient-echo magnitude and phase images were used for quantitative susceptibility mapping (QSM) reconstruction. Magnitude images were used to generate brain masks using brain extraction, and phase images were processed using Laplacian phase unwrapping, VSHARP-based background field removal, and STAR-QSM reconstruction. APART-QSM was then applied to generate paramagnetic susceptibility (χ_{para}) and diamagnetic susceptibility (χ_{dia}) maps. Sub-voxel QSM maps were spatially normalized to Montreal Neurological Institute (MNI) space through

individual T1-weighted images. Smoothed normalized maps were used for voxel-wise statistical analyses, whereas unsmoothed normalized maps were used for regional extraction from substantia nigra (SN) and locus coeruleus (LC) masks. Neuromelanin-sensitive MRI images were rigidly co-registered to individual T1-weighted images. Standard-space SN and LC masks were inverse-transformed into individual T1 native space and applied to the co-registered NM-MRI images for regional signal extraction. QSM, quantitative susceptibility mapping; NM-MRI, neuromelanin-sensitive MRI; mGRE, multi-echo gradient echo; BET, brain extraction tool; VSHARP, variable-kernel sophisticated harmonic artifact reduction for phase data; APART-QSM, anatomic prior-based susceptibility source separation; χ_{para}, paramagnetic susceptibility; χ_{dia}, diamagnetic susceptibility; MNI, Montreal Neurological Institute.

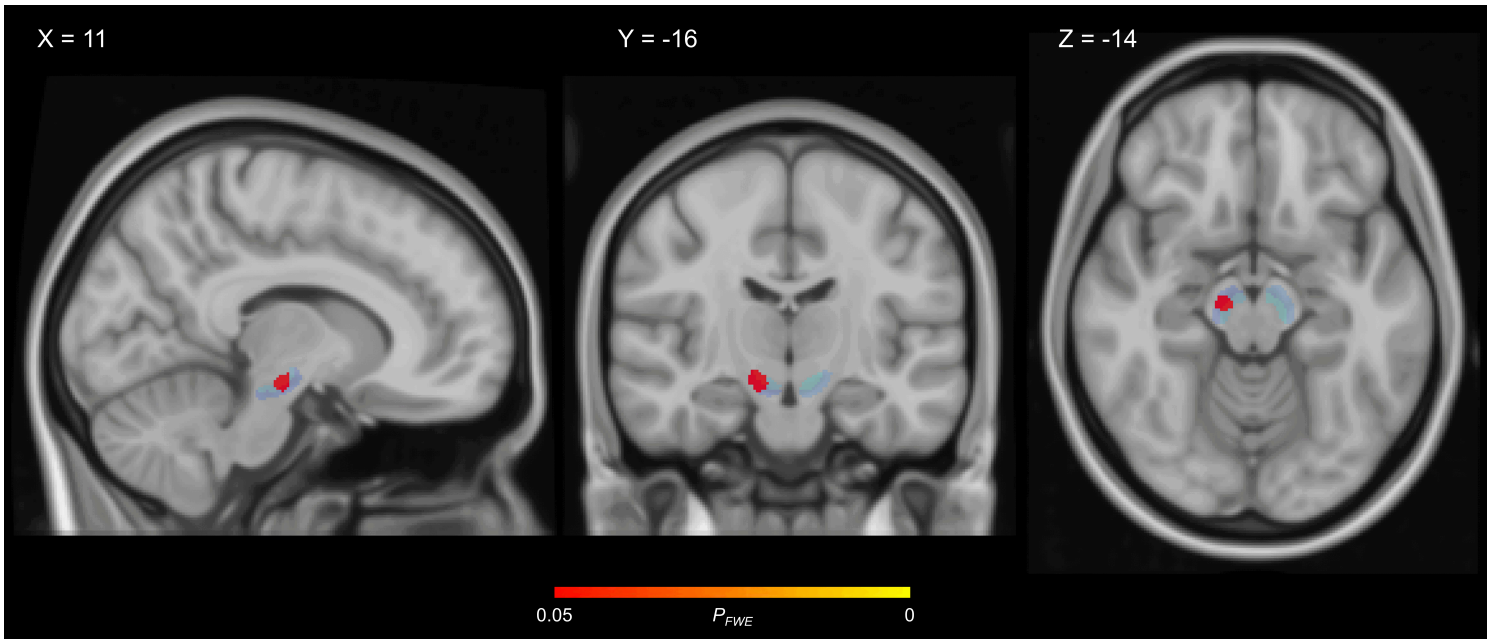


Figure 3

Voxel-wise diamagnetic susceptibility differences among PD sleep phenotypes. Voxel-wise analysis revealed a significant group difference in $|\chi_{dia}|$ within the substantia nigra between patients with PD-SD and those with PD-NSD. Compared with patients with PD-SD, patients with PD-NSD showed higher $|\chi_{dia}|$ values in a significant substantia nigra cluster. Statistical maps are displayed on the standard T1-weighted template at MNI slices x = 11, y = −16, and z = −14. The color bar represents family-wise error-corrected P values. PD, Parkinson's disease; PD-SD, Parkinson's disease with sleep disturbance; PD-NSD, Parkinson's disease without sleep disturbance; SN, substantia nigra; SNpc, substantia nigra pars compacta; SNpr, substantia nigra pars reticulata; χdia, diamagnetic susceptibility; MNI, Montreal Neurological Institute; FWE, family-wise error.

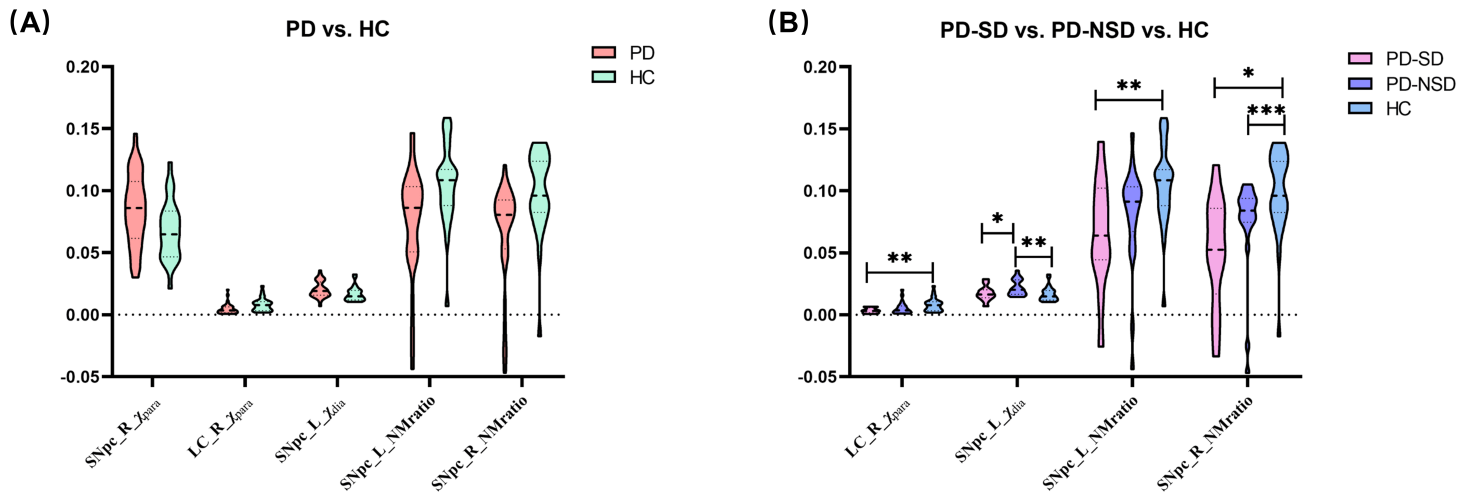


Figure 4

Group differences in susceptibility-derived and neuromelanin-sensitive MRI metrics. Violin plots show group differences in imaging metrics derived from QSM, APART-QSM, and neuromelanin-sensitive MRI. (**A**) Comparisons between patients with PD and HCs. Compared with HCs, patients with PD showed higher χ_{para} in the right SNpc , lower χ_{para} in the right LC, higher $|\chi_{dia}|$ in the left SNpc, and reduced NM ratio in the bilateral SNpc. (**B**) Comparisons among PD-SD, PD-NSD, and HCs. The PD-SD group showed lower right LC χ_{para} than that in HCs. The PD-NSD group showed higher $|\chi_{dia}|$ in the left SNpc than both the PD-SD and HC groups. Bilateral NMratio of SNpc was lower in both PD subgroups than in HCs, with numerically lower values in the PD-SD group. Horizontal lines within each violin indicate the median and interquartile range. *P < 0.05, **P < 0.01, ***P < 0.001. PD, Parkinson's disease; PD-SD, Parkinson's disease with sleep disturbance; PD-NSD, Parkinson's disease without sleep disturbance; HC, healthy control; SNpc, substantia nigra pars compacta; LC, locus coeruleus; χ_{para}, paramagnetic susceptibility; χ_{dia}, diamagnetic susceptibility ; NM ratio, neuromelanin-sensitive contrast ratio.

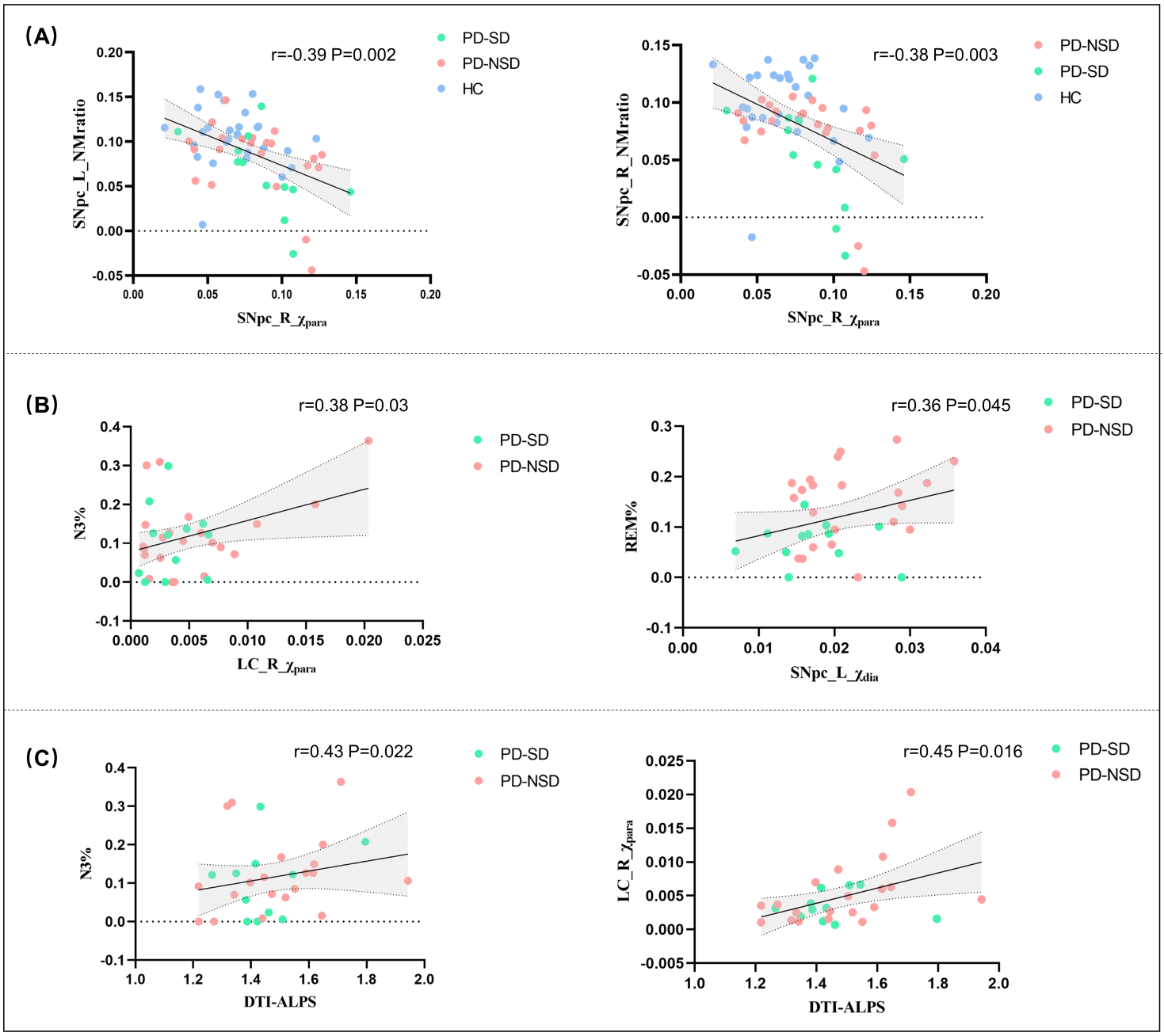


Figure 5

Associations among sub-voxel susceptibility metrics, neuromelanin-sensitive MRI signal, sleep architecture, and glymphatic-related diffusion. Scatter plots show relationships among multimodal imaging markers, polysomnographic sleep parameters, and DTI-ALPS. (**A**) Across all participants, right SNpc paramagnetic susceptibility (χ_{para}) was negatively correlated with left and right SNpc neuromelanin-sensitive contrast ratio (NMratio), indicating an negative association between SNpc paramagnetic susceptibility and neuromelanin-sensitive signal. (**B**) Within the PD cohort, right χ_{para} value of LC was positively correlated with N3 sleep percentage, and left $|\chi_{dia}|$ value of SNpc was positively correlated with REM sleep percentage. (**C**) The DTI-ALPS index was positively correlated with N3 sleep percentage and χ_{para} signal in right LC. Solid lines indicate fitted regression lines, and dotted lines

indicate 95% confidence intervals. PD-SD, Parkinson's disease with sleep disturbance; PD-NSD, Parkinson's disease without sleep disturbance; HC, healthy control; SNpc, substantia nigra pars compacta; LC, locus coeruleus; χ_{para}, paramagnetic susceptibility; χ_{dia}, diamagnetic susceptibility ; NMratio, neuromelanin-sensitive contrast ratio; REM, rapid eye movement sleep; DTI-ALPS, diffusion tensor image analysis along the perivascular space.

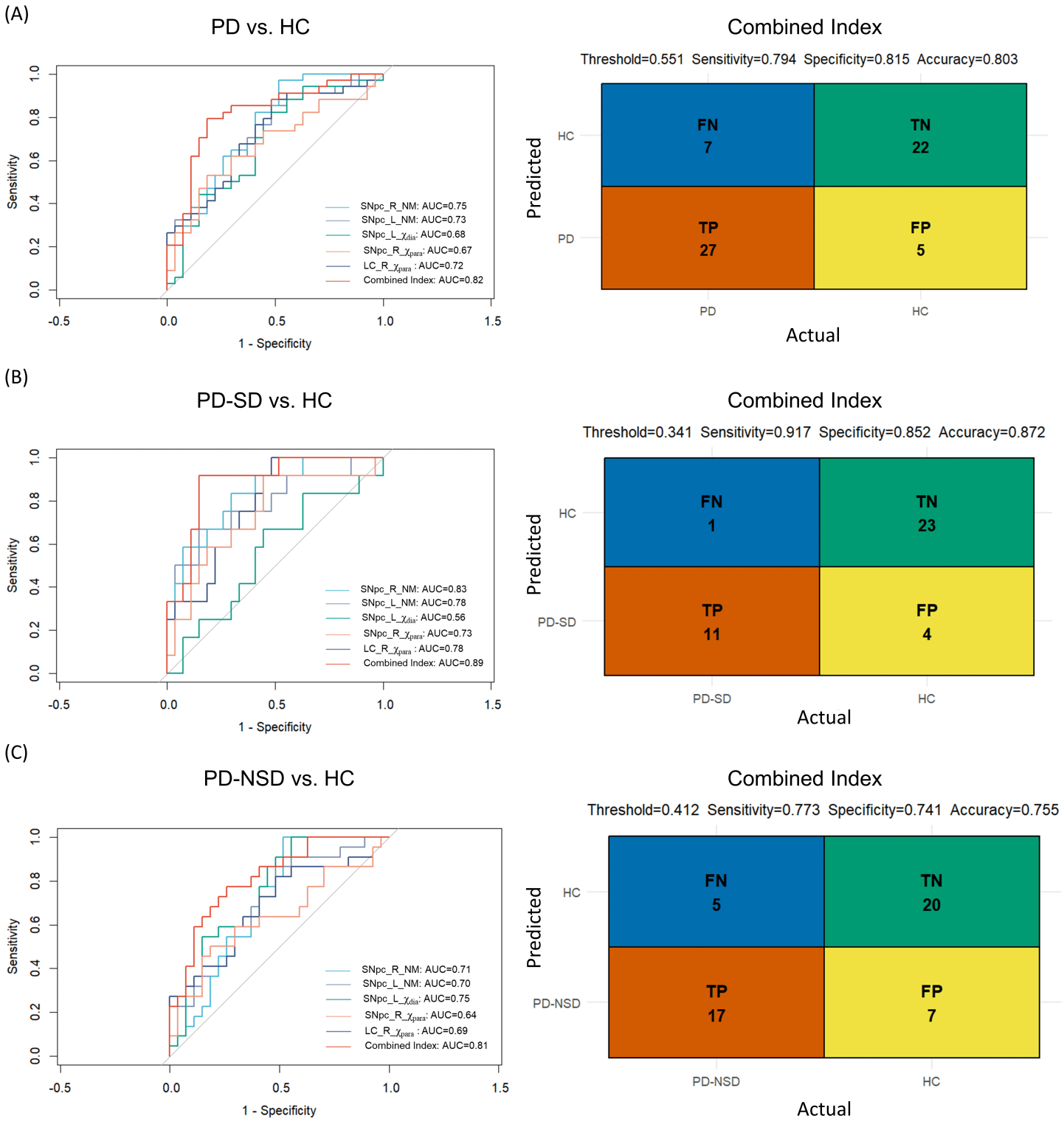


Figure 6

Discriminative performance of individual and combined multimodal MRI markers. Receiver operating characteristic (ROC) curves and confusion matrices show the discriminative performance of sub-voxel QSM and NMratio. (**A**) For discriminating patients with PD from HCs, the combined multimodal index achieved an area under the curve (AUC) of 0.82, with a sensitivity of 79.4%, specificity of 81.5%, and accuracy of 80.3%. (**B**) For discriminating patients with PD-SD from HCs, the combined multimodal index showed the highest apparent discriminative performance, with an AUC of 0.89, sensitivity of 91.7%, specificity of 85.2%, and accuracy of 87.2%. (**C**) For discriminating patients with PD-NSD from HCs, the combined multimodal index achieved an AUC of 0.81, with a sensitivity of 77.3%, specificity of 74.1%, and accuracy of 75.5%. Confusion matrices display the classification results of the combined multimodal index. PD, Parkinson's disease; PD-SD, Parkinson's disease with sleep disturbance; PD-NSD, Parkinson's disease without sleep disturbance; HC, healthy control; ROC, receiver operating characteristic; AUC, area under the curve; SNpc, substantia nigra pars compacta; LC, locus coeruleus; R, right; L, left; χ_{para}, paramagnetic susceptibility; χ_{dia}, diamagnetic susceptibility; NMratio, neuromelanin-sensitive contrast ratio; TP, true positive; TN, true negative; FP, false positive; FN, false negative.

Supplementary Files

This is a list of supplementary files associated with this preprint. Click to download.

- SupplementaryMethods.docx